Diagn Interv Radiol 2026; DOI: 10.4274/dir.2026.263937

NEURORADIOLOGY

REVIEW



# Advancements in magnetic resonance imaging and magnetic resonance-driven techniques for evaluating pituitary macroadenoma consistency: current progress and future perspectives

Chenxin Tian[1#]
Qinglei Shi[2#]
Xinzhi Zhao[2]
Shijia Wang[2]
Junlong Qin[3]
Xuanxun Guo[2]
Ming Feng[1]
Ge Chen[4]
Xiaohai Liu[4]
Renzhi Wang[1,2]

[1]Peking Union Medical College Hospital, Chinese Academy of Medical Science and Peking Union Medical College, Department of Neurosurgery, Beijing, China

[2]Chinese University of Hong Kong (Shenzhen) Faculty of Medicine, Guangdong, China

[3]The Seventh Affiliated Hospital of Southern Medical University, Department of Spine Surgery, Guangdong, China

[4]Xuanwu Hospital Capital Medical University, Department of Neurosurgery, Beijing, China

**#These authors contributed equally to this work.**

**Handling Editor:** Suzan Şaylısoy

**Corresponding author:** Xiaohai Liu

**E-mail:** md-lhxhop@hotmail.com

**Corresponding author:** Renzhi Wang

**E-mail:** wang-rzneuro@hotmail.com

Received 05 March 2026; revision requested 30 March 2026; last revision requested 28 April 2026; accepted 28 May 2026.

Epub: 13.08.2026

DOI: 10.4274/dir.2026.263937

## ABSTRACT

Pituitary macroadenomas (PMAs) are among the most common intracranial tumors and pose significant surgical challenges, especially when the tumor consistency is increased due to high fibrous content. Accurate preoperative assessment of tumor consistency is crucial for optimizing surgical strategies and patient outcomes. Although conventional T2-weighted magnetic resonance imaging (MRI) is widely employed, its predictive value remains uncertain. Emerging techniques, such as diffusion-weighted imaging and magnetic resonance elastography, provide insights into tumor stiffness by assessing microstructural and mechanical properties, enhancing the prediction of PMA consistency. Furthermore, advancements in machine learning (ML) and deep learning, particularly convolutional neural networks (CNNs) and hybrid CNN–transformer models, have improved the extraction of complex imaging features, leading to greater predictive accuracy. This review summarizes recent developments in MRI and MR-driven imaging techniques for predicting PMA consistency, emphasizing their clinical application and the role of ML-based methods in refining predictive models. Despite numerous candidate imaging biomarkers, the field remains constrained by insufficient reproducibility, limited cross-study comparability, heterogeneity in MRI acquisition and post-processing protocols, and poor model generalizability. Continued integration of advanced MRI with ML-driven imaging analyses may further enhance preoperative prediction of PMA consistency and facilitate surgical planning.

## KEYWORDS

Pituitary adenomas, tumor consistency, magnetic resonance imaging, advanced imaging techniques, machine learning

Pituitary adenomas (PAs) represent one of the most prevalent sellar masses, accounting for approximately 10% of all intracranial tumors,[1] with a prevalence of 77.6 cases per 100,000 individuals reported in a recent cross-sectional study.[2] Adenomas measuring ≥ 10 mm are defined as pituitary macroadenomas (PMAs) and constitute approximately 50% of all PAs.[1] Most PAs can be resected through either endoscopic transsphenoidal surgery or the traditional transcranial approach,[3] with the former being preferred due to its minimally invasive nature and reduced complication rates.[3,4] However, the presence of high fibrous content and increased consistency in certain tumors can limit its application.[5] Given their larger size and more prominent imaging characteristics, PMAs have been the primary focus of previous research, providing robust evidence. Thus, preoperative prediction of PMA consistency can aid surgical planning and improve clinical outcomes and patient satisfaction.

Recent advancements in imaging technologies have provided new avenues for predicting tumor consistency preoperatively. It is well-established that T1-weighted magnetic resonance imaging (MRI) is not associated with preoperative assessment of PA consistency.[6] Approximately half of the published studies indicate significant associations between T2-weighted MRI signal intensity (SI) and PA consistency.[7] Diffusion-weighted imaging (DWI) also shows potential, although consensus on the relationship between diffusivity and tumor consistency has not yet been reached.[8] High-resolution DWI methods and emerging MR-driven tech-

You may cite this article as: Tian C, Shi Q, Zhao X, et al. Advancements in magnetic resonance imaging and magnetic resonance-driven techniques for evaluating pituitary macroadenoma consistency: current progress and future perspectives. *Diagn Interv Radiol*. 13 August 2026 DOI: 10.4274/dir.2026.263937 [Epub Ahead of Print].

niques, such as MR elastography (MRE), offer imaging advantages that enhance the accuracy of assessing tissue stiffness and structural properties across various tumor types, including PMAs.

Additionally, machine learning (ML) has substantially improved the capability to extract complex features from imaging data, which were previously challenging to identify and analyze. An increasing number of studies have begun to explore the use of ML to predict neurosurgical outcomes, with encouraging evidence that ML models, particularly those based on MRI, show promise in improving predictive accuracy and aiding clinical decision-making.

Therefore, this review aims to summarize recent advancements in MRI and MR-driven imaging techniques, focusing particularly on studies published from 2000 onward. MRI advancements discussed include conventional T2-weighted MRI, DWI, related diffusion analysis models, MRE, and virtual MRE (vMRE) derived from DWI. Magnetic resonance-driven imaging techniques include radiomics analysis, traditional ML methods, convolutional neural networks (CNNs), and emerging hybrid CNN–transformer models developed based on MR technological advancements. This review examines their roles in the preoperative prediction of PMA consistency and discusses their potential to enhance clinical management of patients with PA (Figure 1).

This study was conducted as a narrative review. We searched the PubMed, Web of Science, and Scopus databases for relevant English-language studies published between 2000 and 2024, using combinations of the following keywords: "pituitary adenoma," "PMA," "tumor consistency," "MRI," "DWI," "ADC," "MRE," "radiomics," "ML," and "deep learning." Studies relevant to the preoperative imaging assessment of PMA consistency were prioritized. Additional articles were identified through a manual review of reference lists. Given the heterogeneity in imaging protocols, definitions of consistency, and study endpoints across available literature, a narrative review format was deemed appropriate for summarizing current evidence and highlighting directions for future research.

## Clinical importance of preoperative assessment of pituitary macroadenoma consistency

Preoperative assessment of PMA consistency is critical for optimizing surgical outcomes, guiding operative strategies, and enhancing patient care. Consistency, referring to the tumor's firmness or texture, directly influences surgical approaches, extent of resection (EOR), and associated complications.

The firmness of a PA considerably affects surgical difficulty. Studies by Rutkowski et al.[9] and Acitores Cancela et al.[10] emphasize that soft tumors are typically easier to aspirate and remove, frequently resulting in higher EORs. In contrast, fibrous tumors pose substantial challenges due to their firm texture, often necessitating additional surgical tools or specialized techniques, such as extracapsular dissection. Fibrous tumors are also associated with prolonged operative times, increased rates of intraoperative cerebrospinal fluid (CSF) leaks, and lower gross total resection (GTR) rates. One study reported a GTR rate of 76.3% for soft tumors compared with 48.7% for fibrous tumors, demonstrating the significant clinical impact of tumor consistency on surgical outcomes.[10] Representative intraoperative endoscopic images further illustrate the differences in tumor consistency and related surgical implications (Figure 2).

Pituitary adenoma consistency also correlates with postoperative outcomes and complications. Fibrous tumors have higher complication rates, including hypopituitarism, permanent diabetes insipidus, and the need for postoperative radiotherapy. A recent study demonstrated that fibrous tumors carry an 8.57-fold increased risk of postoperative hormone deficiencies compared with soft tumors, likely due to difficulties in achieving complete resection. Additionally, harder tumors more commonly leave residual tissue, resulting in higher recurrence rates and the need for subsequent interventions.[11]

Tumor consistency is closely related to the biological characteristics of PAs. Harder tumors generally exhibit higher collagen content, particularly types I and III.

### Main points

- Integration of magnetic resonance imaging (MRI) and machine learning (ML)-based image analysis shows considerable potential for predicting pituitary macroadenoma (PMA) consistency and enhancing preoperative planning.
- This review summarizes recent advances in MRI and MR-driven imaging techniques for predicting the consistency of PMAs.
- The clinical applications of these methods and the role of ML-based approaches in refining predictive models are highlighted.
- Additional techniques, including diffusion-weighted imaging and magnetic resonance elastography, offer valuable insights into tumor stiffness.

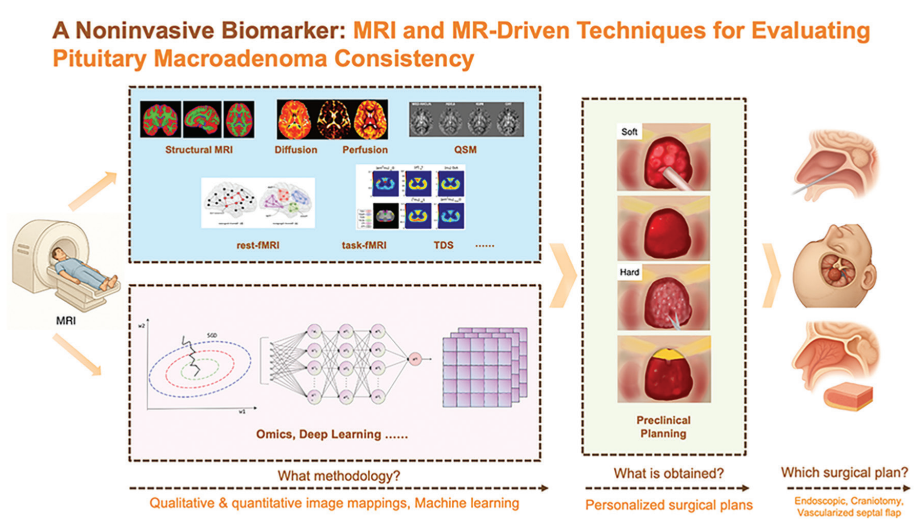


**Figure 1.** A non-invasive imaging and machine learning framework for predicting pituitary macroadenoma consistency and personalizing surgical strategies. Graphical abstract illustrating a comprehensive framework for non-invasively assessing the consistency of pituitary macroadenomas using multimodal magnetic resonance imaging (MRI) and advanced machine learning techniques. Structural MRI, diffusion-weighted imaging, magnetic resonance elastography, and other advanced imaging modalities provide rich information about tumor microstructure and mechanical properties. These data are processed using deep learning and radiomics methods—such as convolutional neural networks, transformer-based models, and omics analysis—to extract predictive features related to tumor stiffness. The resulting classification into "soft" or "hard" tumors informs personalized preoperative planning and helps determine the optimal surgical approach (e.g., endoscopic resection, craniotomy, vascularized septal flap reconstruction). This workflow supports the use of tumor consistency as a clinically actionable imaging-derived biomarker to guide safer and more effective treatment strategies.

These tumors often show stronger associations with cavernous sinus invasion and suprasellar extension, complicating surgical resection due to the intricate anatomy of these regions.[12] Yao et al.[13] highlighted that vascularity tends to be higher in softer tumors, whereas firmer tumors demonstrate reduced vascularity. Although few studies explicitly investigate the relationship between tumor consistency and perfusion in PAs, evidence from other tumor types, including meningiomas, gliomas, liver cancers, and neuroblastomas, suggests that stiffness and vascularity influence each other and affect clinical outcomes.

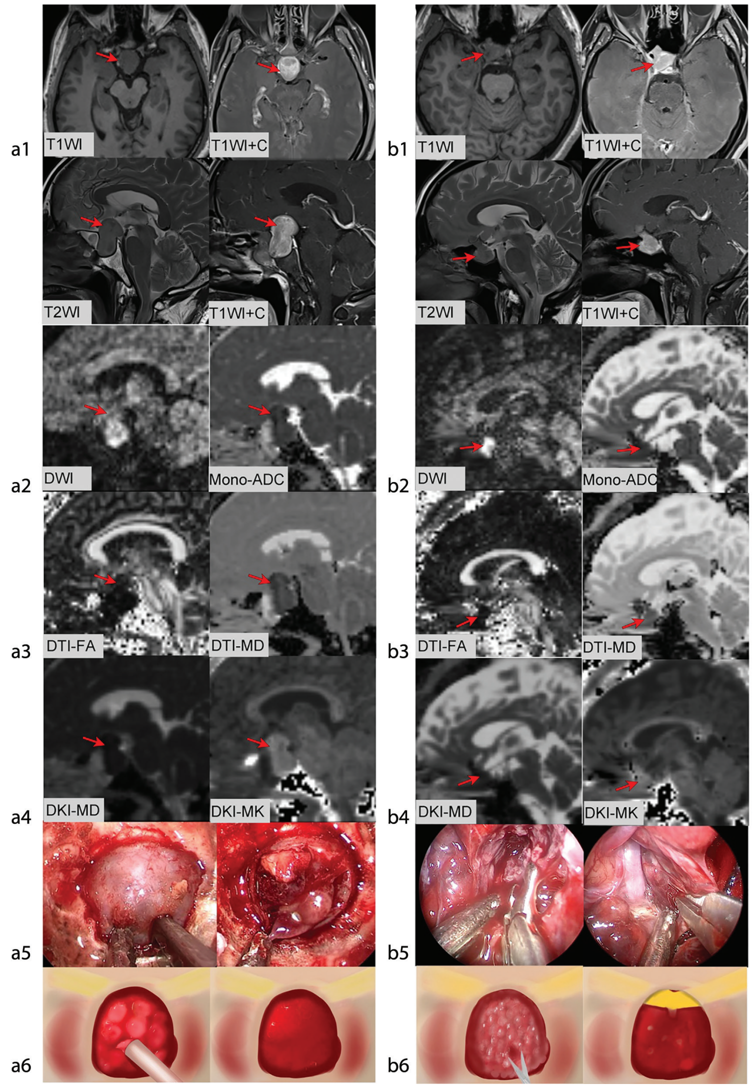


**Figure 2.** Comparative multimodal magnetic resonance imaging and intraoperative features of two pituitary macroadenomas with distinct tumor consistencies. Red arrows in a1–b4 indicate the tumor locations on each imaging sequence. See Supplementary Table 1 for corresponding quantitative imaging values [apparent diffusion coefficient (ADC), diffusion tensor imaging, diffusion kurtosis imaging] for the soft and hard tumors. Left column (a1–a6): soft-consistency pituitary macroadenoma.

a1) Conventional anatomical imaging shows a large intrasellar–suprasellar mass with well-defined borders and homogeneous signal intensity.

a2) Diffusion-weighted imaging (DWI) and mono-exponential ADC maps demonstrate hyperintensity on DWI and high ADC values, consistent with facilitated diffusion.

a3) Diffusion tensor imaging shows elevated fractional anisotropy (FA) and mean diffusivity (MD), suggesting low cellular density and preserved microstructure.

a4) Diffusion kurtosis imaging reveals low DKI-derived MD and mean kurtosis (MK) values, indicating low tissue complexity and mechanical softness.

a5) Intraoperative photographs show a soft tumor easily aspirated with a suction device, with an intact sellar diaphragm and no cerebrospinal fluid (CSF) leakage.

a6) Schematic illustration showing smooth tumor aspiration and preserved diaphragm.

Right column (b1–b6): hard-consistency pituitary macroadenoma.

b1) Anatomical MRI reveals a heterogeneous, lobulated tumor extending beyond the sella.

b2) Diffusion-weighted imaging shows restricted diffusion and low ADC values, indicative of higher cellularity.

b3) Diffusion tensor imaging maps demonstrate disrupted diffusion architecture with low MD and altered FA.

b4) Diffusion kurtosis imaging analysis shows elevated MK, reflecting complex, fibrotic microstructure.

b5) Intraoperative findings depict a firm, fibrous tumor requiring piecemeal debulking and sharp dissection. Postoperatively, diaphragmatic disruption and CSF leakage occurred, necessitating fascia and fat graft reconstruction.

b6) Schematic shows tumor resistance to suction and exposure of suprasellar structures post-resection.

Figure 2 illustrates two representative PMA cases with markedly different intraoperative consistencies: one soft and easily aspirated, the other firm, fibrous, and surgically challenging. Multimodal MRI sequences, including DWI, apparent diffusion coefficient (ADC), diffusion tensor imaging (DTI), and diffusion kurtosis imaging (DKI), demonstrate measurable imaging differences between these two cases that correlate with their surgical outcomes (Supplementary Table 1). The hard tumor exhibited restricted diffusion and elevated kurtosis, consistent with dense collagenous stroma, necessitating prolonged operative time, subtotal resection, and postoperative CSF leakage repair (Supplementary Figure 1). These cases visually and quantitatively highlight the predictive value of advanced imaging in preoperative consistency assessment, reinforcing the importance of incorporating these techniques into clinical decision-making.

## Magnetic resonance imaging methods in tumor consistency evaluation: qualitative approaches

Despite advancements in imaging technologies, evaluating tumor consistency remains challenging using traditional MRI techniques, which can be broadly categorized into qualitative and quantitative assessments. Qualitative approaches, such as T1- and T2-weighted MRI, emphasize morphological characteristics, whereas quantitative methods, including DWI and MRE, assess functional tissue properties. Additionally, advanced imaging technologies, such as high-resolution DWI, enhance image quality and provide greater detail for consistency evaluation. These methods collectively demonstrate potential for improving the preoperative assessment of PA consistency.

### Traditional T1- and T2-weighted magnetic resonance imaging

MRI is routinely employed in PA imaging. On T1- and T2-weighted MRI sequences, the anterior pituitary gland exhibits isointensity similar to gray matter, whereas the posterior pituitary gland demonstrates high SI on T1-weighted sequences and low SI on T2-weighted sequences. Contrast-enhanced MRI sequences can facilitate the detection of PAs that are otherwise difficult to visualize. Gadolinium-based contrast agents (GBCAs) are widely used for PAs; however, they tend to deposit in the basal ganglia and other brain regions.[14] Thus, current consensus guidelines recommend careful consideration regarding repeated postoperative follow-up imaging, as neurosurgeons must remain aware of potential risks associated with multiple GBCA exposures.[14] For assessing the extent of cavernous sinus invasion by macroadenomas, the Knosp classification on coronal MRI is commonly applied. Higher Knosp grades indicate greater cavernous sinus invasion and lower GTR likelihood[15,16] Grades 3A and 3B distinguish outcomes between superior and inferior cavernous sinus invasions, whereas Grade 4 tumors, fully encasing the intracavernous internal carotid artery, rarely achieve GTR.[16]

The use of T2-weighted MRI in evaluating PA consistency has been extensively studied over the past two decades; however, findings remain inconsistent and methodologically diverse (Table 1). Most studies assessed tu-

**Table 1.** Studies using T2-weighted MRI to assess pituitary tumor consistency, from the year 2000 to the year 2024

| Author | Year | Sample size | Imaging parameters and analysis metrics | Conclusion |
|---|---|---|---|---|
| **Baban**[67] | 2024 | 68 | Axial, sagittal, coronal, tumor/pons | No significant results |
| **Gaia**[68] | 2022 | 15 | 1.5T, axial, sagittal, coronal, 3-mm thickness, tumor/white matter | No significant results |
| **Li**[12] | 2021 | 55 | 3.0T, tumor/pons | No significant results |
| **Kamimura**[38] | 2021 | 49 | 3.0T, coronal | No significant results |
| **Chen**[20] | 2020 | 191 | 1.5T, axial, tumor/cerebellar peduncle | Fibrous tumors showed lower SI |
| **Yun**[7] | 2020 | 50 | Coronal, tumor/pons | Fibrous tumors showed lower SI |
| **Yao**[13] | 2020 | 15 | 7.0T, coronal, 2-mm thickness, tumor/gray matter | No significant results |
| **Mastorakos**[19] | 2019 | 196 | Axial and coronal, tumor/cerebellar peduncle | No significant results |
| **Cappelletti**[69] | 2019 | 66 | Coronal | No significant results |
| **De Araujo e Silva**[17] | 2017 | 35 | Axial, tumor/cerebellar peduncles | Fibrous tumors showed lower SI |
| **Taghvaei**[35] | 2017 | 45 | 3.0T, axial and coronal, 3-mm thickness, tumor/white matter | No significant results |
| **Thotakura**[70] | 2017 | 100 | 1.5T, tumor/white matter | No significant results |
| **Yiping**[41] | 2016 | 34 | 3.0T, coronal, 3-mm thickness, tumor/white matter | No significant results |
| **Wei**[21] | 2015 | 38 | 3.0T, 1-mm thickness, tumor/pons | Fibrous tumors showed lower SI |
| **Smith**[22] | 2015 | 36 | Axial | Fibrous tumors showed lower SI |
| **Alimohamadi**[71] | 2014 | 30 | 1.5T, axial, sagittal, coronal, 3-mm thickness, tumor/white matter | No significant results |
| **Mahmoud**[42] | 2011 | 24 | 3.0T, coronal, 3-mm thickness, tumor/white matter | No significant results |
| **Boxerman**[72] | 2010 | 28 | 1.5T, axial, tumor/pons, 5-mm thickness | No significant results |
| **Suzuki**[37] | 2007 | 19 | 1.5T, coronal, 3-mm thickness | Fibrous tumors showed higher SI |
| **Bahuleyan**[73] | 2006 | 80 | 0.5T, coronal, 3-mm thickness | No significant results |
| **Pierallini**[31] | 2006 | 22 | 1.5T, coronal, 3-mm thickness, tumor/white matter | Fibrous tumors showed higher SI |
| **Hagiwara**[74] | 2003 | 174 | 1.0T or 1.5T, coronal, 3-mm thickness, tumor/white matter | No significant results |
| **Naganuma**[5] | 2002 | 66 | | Fibrous tumors were isointense on T2 |

MRI, magnetic resonance imaging; SI, signal intensity.

mor SI qualitatively or by calculating the ratio between the mean SI of the tumor and that of reference structures, such as white matter, the pons, or cerebellar peduncles.[6,17-19] Several studies report that fibrous PAs exhibit lower SI on T2-weighted images than non-fibrous tumors.[7,17,20-22] In contrast, other reports describe fibrous lesions as hyperintense or isointense, or find no significant association between T2 SI and tumor consistency. This variability likely reflects methodological heterogeneity across studies, including differences in region-of-interest (ROI) definitions, reference tissue selections for signal normalization, MRI acquisition parameters (e.g., field strength, slice thickness, image orientation), and variation in surgical or histopathological standards for defining tumor consistency. Therefore, although T2-weighted imaging may provide supportive information regarding tumor characteristics, its standalone predictive value for PA consistency remains limited for reliable clinical decision-making. Future studies should prioritize standardizing protocols and integrating advanced MRI techniques with ML-based models to enhance predictive accuracy.

In addition, fast imaging employing steady-state acquisition (FIESTA) and its related sequence, constructive interference in steady-state, are MRI techniques providing high-resolution imaging with superior contrast for visualizing small structures and tissue interfaces. Their capability to delineate fine structural details and intratumoral characteristics has significant implications for predicting tumor consistency. Particularly, contrast-enhanced FIESTA (CE-FIESTA) has demonstrated potential in distinguishing between soft and hard PAs by identifying SI patterns correlated with collagen content and tumor stiffness. Yamamoto et al.[23] classified PAs in 29 patients into solid or mosaic types based on CE-FIESTA imaging. Solid-type tumors exhibited homogeneous SI without intratumoral hyperintense dots, corresponding to harder consistency, higher collagen content, and smaller postoperative tumor size. Conversely, mosaic-type PAs, characterized by intratumoral hyperintense dots, were softer with lower collagen content. Statistical analyses confirmed that CE-FIESTA had significantly higher sensitivity and specificity for predicting tumor consistency than conventional T1- and T2-weighted sequences.

## Magnetic resonance imaging methods in tumor consistency evaluation: quantitative approaches

Although qualitative, morphology-based imaging provides a useful foundation, its impact on assessing tissue composition remains limited. Consequently, quantitative methods have gained increased attention due to their potential to offer functional insights into tumor consistency.

### Conventional mono-exponential diffusion-weighted imaging

DWI measures the diffusion of water molecules within tissues, providing insights into tumor microstructure by reflecting the cellular environment's influence on water mobility.[24] In tumors, cellular density, extracellular matrix composition, and cell membrane integrity all affect water diffusion. Soft tumors, typically characterized by lower cell density and a less rigid extracellular matrix, generally exhibit higher diffusion, whereas harder tumors with compact, fibrous structures show restricted diffusion. Thus, DWI can effectively evaluate structural characteristics of PAs, particularly regarding tumor consistency.[24]

The conventional mono-exponential DWI model is widely used due to its simplicity and clinical applicability. A simplified representation of the diffusion imaging mechanism is shown in Figure 3. This approach assumes water diffusion follows a Gaussian distribution, modeling diffusion-weighted signal decay as an exponential function of the *b*-value:

$$S(b) = S_0 \cdot e^{-b \cdot ADC}$$

Here, *S(b)* is the SI at a given *b*-value, $S_0$ is the SI without diffusion weighting (*b=0*), and ADC is the apparent diffusion coefficient.[25-27] The ADC provides a single quantitative measure of diffusion, with lower ADC values reflecting restricted diffusion (e.g., in denser or fibrous tumors) and higher ADC values indicating increased water mobility (e.g., in softer tumors).[24]

The application of DWI and ADC as non-invasive tools for evaluating PA consistency has been extensively investigated; however, the available evidence remains inconsistent (Table 2). Several studies reported lower ADC values in fibrous tumors, supporting the hypothesis that increased extracellular matrix components, such as collagen or reticulin, restrict water diffusion.[21,28-30] From a surgical perspective, these firmer tumors are typically more challenging to resect, supporting the biological plausibility of the association between restricted diffusion and tumor firmness. However, other studies have described higher ADC values in fibrous tumors,[31-34] and many have found no significant correlation between DWI/ADC parameters and adenoma consistency.[35-42] These discrepant findings likely reflect both biological complexity and methodological differences across studies. Diffusion measurements can be influenced by MRI acquisition parameters, ROI definitions, and variations in the reference standard for tumor consistency. Additionally, measurements may be affected by complex interactions among extracellular matrix composition, tumor cellularity, microvascular perfusion, and intratumoral factors, such as cystic, necrotic, or hemorrhagic changes. Moreover, conventional DWI employs a mono-exponential diffusion model, which cannot effectively differentiate true molecular diffusion from perfusion effects

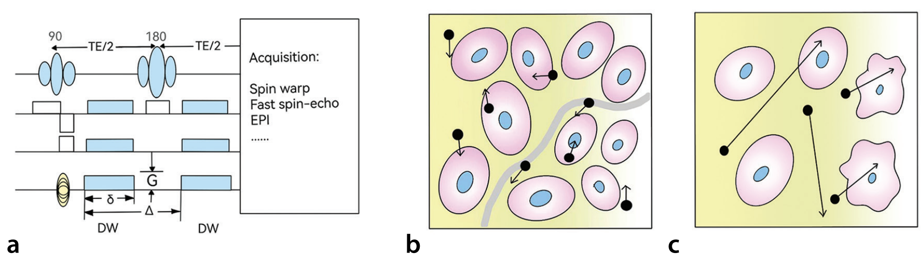


**Figure 3.** Principle mechanism of diffusion-weighted imaging. **(a)** A typical mechanism for diffusion imaging, obtained from Moritani, Ekholm, and Westesson, Diffusion-Weighted MR Imaging of the Brain.[27] During the time evolution, a pair of diffusion-encoding gradients is applied (fourth row), each with a duration *δ*, an amplitude *G* (usually in mT/m), and separated by an interval *Δ*. These gradients encode molecular diffusion by inducing phase shifts in moving water protons. Reduced diffusion leads to less dephasing and hence higher signal. Greater values of *δ*, *G*, or *Δ* enhance the sensitivity to diffusion, as greater *δ* means longer duration of the diffusion encoding gradients, greater *G* means stronger diffusion encoding gradients, and greater *Δ* means longer intervals for water molecules to diffuse to other places. **(b)** Restricted diffusion: In tissues with high cellularity and intact cell membranes, water diffusion is restricted, resulting in low diffusivity and high signal intensity (SI) on diffusion-weighted imaging (DWI). The densely packed cells and blood vessels limit extracellular space and reduce water mobility. **(c)** Free diffusion: In tissues with low cellularity and defective cell membranes, the relative increase in extracellular space allows free movement of water molecules between extracellular and intracellular spaces, yielding higher diffusivity and lower SI on DWI. Panels B and C are adapted from Koh and Collins, Diffusion-Weighted MRI in the Body.[78]

Table 2. Studies using conventional mono-exponential models to assess pituitary tumor consistency, from the year 2000 to the year 2024

| Author | Year | Sample size | Imaging parameters and analysis metrics | Conclusion |
|---|---|---|---|---|
| **Barbosa**[36] | 2024 | 80 | 1.5T, coronal, 3-mm thickness, *b* values 0 and 1000 sec/mm$^2$, tumor/pons | No significant results |
| **Ding**[28] | 2021 | 183 | 3.0T, axial, 4-mm thickness, *b* values 1000 sec/mm$^2$, tumor/brainstem | Fibrous tumors showed lower ADC values |
| **Kamimura**[38] | 2021 | 49 | 3.0T, coronal, 2-mm thickness, *b* values 0 and 1000 sec/mm$^2$, tumor/white matter | No significant results |
| **Cohen-Cohen**[39] | 2021 | 38 | 3.0T, coronal and axial, 3-mm thickness, tumor/white matter | No significant results |
| **Su**[30] | 2020 | 15 | 3.0T, coronal, 3-mm thickness, *b* values 1000 and 2000 sec/mm$^2$ | Fibrous tumors showed lower ADC values |
| **Rutland**[29] | 2021 | 13 | 7.0T, coronal, *b* values 1200 sec/mm$^2$, tumor/gray matter | Fibrous tumors showed lower ADC values |
| **Alimohamadi**[75] | 2019 | 16 | 1.5T, axial, 5-mm thickness, *b* values 0 and 1000 sec/mm$^2$, tumor/white matter | Fibrous tumors showed restricted diffusion |
| **Garg**[40] | 2019 | 33 | 3.0T, 6-mm thickness, *b* values 0 and 1000 sec/mm$^2$ | No significant results |
| **Alashwah**[33] | 2017 | 20 | 1.5T, axial, 6-mm thickness, *b* values 0, 500, 1000 sec/mm$^2$ | Fibrous tumors showed higher ADC values |
| **Taghvaei**[35] | 2017 | 45 | 3.0T, axial and coronal, 3-mm thickness, *b* values 0, 1000, 3000, 5000 sec/mm$^2$, tumor/white matter | No significant results |
| **Yiping**[41] | 2016 | 34 | 3.0T, coronal, 3-mm thickness, tumor/brainstem | No significant results |
| **Wei**[21] | 2015 | 38 | 3.0T, *b* values 100 sec/mm$^2$, tumor/pons | Fibrous tumors showed lower ADC values |
| **Thomas**[34] | 2014 | 31 | Axial, tumor/white matter | Fibrous tumors showed higher ADC values |
| **Alimohamadi**[71] | 2014 | 30 | 1.5T, axial, sagittal, coronal, tumor/white matter | No significant results in ADC values; fibrous tumors showed lower DWI SI |
| **Mohamed**[32] | 2013 | 30 | 1.5T, axial, 6-mm thickness, *b* values 0 and 1000 sec/mm$^2$ | Fibrous tumors showed higher ADC values |
| **Mahmoud**[42] | 2011 | 24 | PROPELLER DWI, 3.0T, coronal, 4-mm thickness, *b* values 0 and 1000 sec/mm$^2$, tumor/white matter | No significant results |
| **Boxerman**[72] | 2010 | 28 | 1.5T, axial, 5-mm thickness, *b* values 0 and 1000 sec/mm$^2$, tumor/pons | Fibrous tumors showed lower ADC values |
| **Suzuki**[37] | 2007 | 19 | 1.5T, coronal, 3-mm thickness, *b* values 5 and 1000 sec/mm$^2$ | No significant results |
| **Pierallini**[31] | 2006 | 22 | 1.5T, coronal, 5-mm thickness, acquisition time 32 seconds, *b* values 0 and 1000 sec/mm$^2$, tumor/white matter | Fibrous tumors showed higher ADC values; no significant results in DWI SI |

SI, signal intensity; ADC, apparent diffusion coefficient; DWI, diffusion-weighted imaging.

or accurately represent tissue heterogeneity. Therefore, although ADC provides useful quantitative information, it should currently be viewed as a supportive yet non-specific marker, rather than a definitive biomarker of tumor consistency. These limitations have led to increased interest in advanced diffusion modeling techniques, especially those based on optimized multi-*b*-value acquisitions, such as intravoxel incoherent motion (IVIM), DKI, diffusion spectrum imaging, and mean apparent propagator-MRI. These methods offer a more comprehensive characterization of PA microstructure and may enhance future preoperative assessments of tumor consistency.

## Other advanced diffusion-weighted imaging models

Advanced diffusion models, including IVIM, address limitations of the mono-exponential model by incorporating additional parameters that reflect more complex biological processes. IVIM separates the diffusion signal into two components: molecular diffusion (slow component) and microvascular perfusion (fast component). The IVIM model is expressed as:

$$S(b) = S_0 \cdot [f \cdot e^{-bD^*} + (1-f) \cdot e^{-bD}]$$

Here, $D$ represents the diffusion coefficient (true molecular diffusion), D* is the pseudo-diffusion coefficient (perfusion-related diffusion), and $f$ is the perfusion fraction (signal proportion from perfusion).[43] By distinguishing these components, IVIM provides insights into tissue microstructure and vascular characteristics. Furthermore, IVIM can convert ADC values into virtual stiffness values, potentially enhancing assessments when combined with other MR techniques.

Diffusion–relaxation correlation spectrum imaging (DR-CSI) is an advanced, multidimensional DWI technique that simultaneously captures diffusion and T2 relaxation properties by acquiring SIs over various *b*-values and echo times. Unlike conventional DWI or T2 mapping, DR-CSI constructs a voxel-wise spectrum representing complex tissue microenvironments, allowing detection of subtle heterogeneity at a sub-voxel level. In assessing PMA consistency, DR-CSI enables non-invasive quantification of microstructural features such as cellularity, water content, and fibrosis by generating voxel-wise DR spectra. A spectral component characterized by intermediate diffusivity and short T2 was found significantly elevated in harder tumors, correlating with increased collagen content on histology. Conversely, a component with intermediate diffusivity and longer T2 was more prominent in softer tumors, likely reflecting higher water content or cystic changes.[44] These findings highlight DR-CSI's capability to differentiate soft from firm PMAs based on imaging biomarkers reflective of underlying histopathological consistency.

### High resolution diffusion-weighted imaging

High-resolution DWI improves spatial resolution, reduces magnetic susceptibility artifacts and image distortion, provides more detailed anatomical information, reduces partial volume effects, and thus enhances diagnostic value. Reduced field of view DWI is an optimized technique that narrows the scanning field in the phase-encoding direction, minimizing distortions and improving spatial resolution; this is especially beneficial in areas prone to susceptibility artifacts, such as the sellar region. With this technique, tumor diffusivity assessment in PMAs can be enhanced through clearer images and more reliable ADC measurements, improving predictions of PMA consistency based on differences in SI between soft and hard tumors.[45]

Turbo spin-echo DWI (TSE-DWI) employs repeated 180° refocusing pulses after the initial 90° excitation pulse. This approach reduces susceptibility-induced distortions and artifacts common near air–tissue interfaces, such as the paranasal sinuses.[46] In PMA evaluation, TSE-DWI provides clearer visualization of the pituitary gland and adjacent structures, which is crucial for assessing tumor consistency. Studies indicate that TSE-DWI achieves superior image quality and more accurate ADC measurements compared with conventional DWI.[46] The reduced artifacts and improved spatial resolution of TSE-DWI make it a valuable method for accurately assessing pituitary lesions, particularly in anatomically challenging regions.

### Magnetic resonance elastography and virtual magnetic resonance elastography

Magnetic resonance elastography has emerged as a promising method for assessing PA consistency preoperatively, providing non-invasive insights into tumor stiffness essential for surgical planning. The MRE process involves three key steps: generating mechanical waves within tissue, capturing these waves using MRI, and processing the data to produce elastograms. A mechanical actuator introduces low-frequency vibrations into tissue, which propagate as shear waves. Stiffer tissues cause faster wave propagation due to their microstructural properties. MRI sequences, typically gradient-echo or spin-echo, are synchronized with vibration frequency to capture wave patterns. The wave data are then processed using an inversion algorithm to quantify tissue stiffness.

Magnetic resonance elastography is particularly valuable for identifying fibrosis and other pathological tissue changes. It can differentiate between soft, intermediate, and firm tumors, substantially influencing the technical difficulty, duration, and complication risks of transsphenoidal resections. Hughes et al.[47] demonstrated that MRE distinguished soft from intermediate PMAs, with mean stiffness values of 1.38 kPa for soft tumors and 1.94 kPa for intermediate tumors. Sakai et al.[48] reported significant correlations between MRE-derived stiffness values and intraoperative consistency across various intracranial tumors, including PMAs. Similarly, Cohen-Cohen et al.[39] showed that absolute and relative stiffness values from MRE correlated significantly with intraoperative consistency. This study highlighted that firmer tumors were associated with longer operative times and higher complication rates, reinforcing the clinical relevance of preoperative MRE for patient counseling and surgical optimization.

Magnetic resonance elastography combined with DTI represents an emerging imaging approach designed to non-invasively characterize both mechanical and microstructural properties of intracranial tumors. Magnetic resonance elastography measures tissue stiffness by tracking mechanical shear-wave propagation, and DTI evaluates tissue architecture and anisotropy through water diffusion patterns within tumors. A study on meningiomas found that combining MRE and DTI significantly improved preoperative consistency prediction accuracy [area under the receiver operating characteristic curve (AUC): 0.88], with histological findings correlating tumor firmness to cell density and fibrous content. Although the study focused on meningiomas, combining biomechanical stiffness from MRE and structural anisotropy from DTI is relevant for PMAs, where tumor consistency similarly impacts surgical difficulty. Therefore, applying MRE–DTI to PMAs could offer a powerful non-invasive tool for predicting tumor firmness, optimizing resection strategies, and reducing operative complications.[49]

Although MRE shows potential for evaluating PA consistency, its technical complexity, requirement for specialized equipment, and high costs limit routine clinical accessibility. vMRE, introduced by Lagerstrand et al.,[50] utilizes DWI techniques such as IVIM to generate parameter maps resembling elastography images, enabling stiffness assessment without mechanical vibrations. This approach is non-invasive, straightforward, cost-effective, and easy to implement, presenting a promising clinical alternative (Figure 4). vMRE uses DWI-derived data instead of physical vibrations and applies mathematical models to convert ADC values into virtual stiffness measurements. By eliminating mechanical actuators, vMRE improves patient comfort and accessibility while still providing reliable tissue elasticity assessments.

Compared with conventional MRI and standard DWI, MRE aligns more closely mechanistically with the concept of tumor stiffness. It may therefore have greater biological relevance for evaluating PA consistency. Aunan-Diop et al.[51] suggested that although MRE remains at a preclinical stage, it shows promise for assessing tumor consistency, adhesion, and mechanical heterogeneity in intracranial neoplasms. Studies by Le Bihan et al.[25,26,52] demonstrated a significant correlation ($r^{2:}$ 0.90) between MRE-derived stiffness and shifted ADC values in liver tissues. These findings support the conceptual feasibility of vMRE as a non-vibration-based alternative. Ota et al.[53] extended this application to liver tumors, showing that combining MRE and vMRE improved the differentiation of hepatocellular carcinoma from metastases, achieving higher sensitivity and specificity than with MRE alone. Jung et al.[54] applied vMRE to differentiate benign from metastatic cervical lymph nodes in head and neck cancers, obtaining considerable diagnostic accuracy based on elasticity values. However, these supporting data are primarily derived from non-pituitary tissues, making their applicability to PMAs uncertain due to differences in anatomical location, tumor composition, and biomechanical environment. Consequently, the potential role of vMRE in PMA consistency assessment should currently be viewed as theoretical and extrapolative, rather than directly validated. Moreover, the evidence for elastography-based techniques in this area remains limited by small sample sizes, specialized hardware requirements, restricted availability, and lack of standardized acquisition and post-processing protocols. Therefore, MRE represents a promising investigational approach for preoperative stiffness assessment, and vMRE remains a hypothesis-generating technique requiring validation in dedicated pituitary studies before clinical application can be considered.

### Magnetic resonance imaging-based machine learning techniques in predicting pituitary adenoma consistency

The application of ML for predicting PA consistency can be classified into three types based on methodology: traditional ML methods, CNNs, and transformer-based neural networks. The current status of these methods will be introduced based on advancements in MR imaging.

## Radiomics and conventional machine learning in pituitary adenoma consistency evaluation

Traditional ML algorithms include various approaches that were widely utilized before the emergence of deep learning. These methods depend on logical reasoning, expert systems, shallow model structures, and explicit feature extraction. Traditional ML typically involves several steps: image acquisition and reconstruction, ROI segmentation, feature extraction, feature selection, and modeling[55] (Figure 5). High-quality MRI data form the basis for image acquisition. Regions of interest are usually segmented manually or automatically, defining the tumor region for further analysis. From these ROIs, radiomic features, including first-order (like intensity), second-order (like texture), and higher-order, are extracted. Feature selection techniques, such as reproducibility analysis, dimensionality reduction, and ML algorithms, identify the most relevant features while reducing redundancy. Finally, predictive models are developed using classifiers to estimate clinical

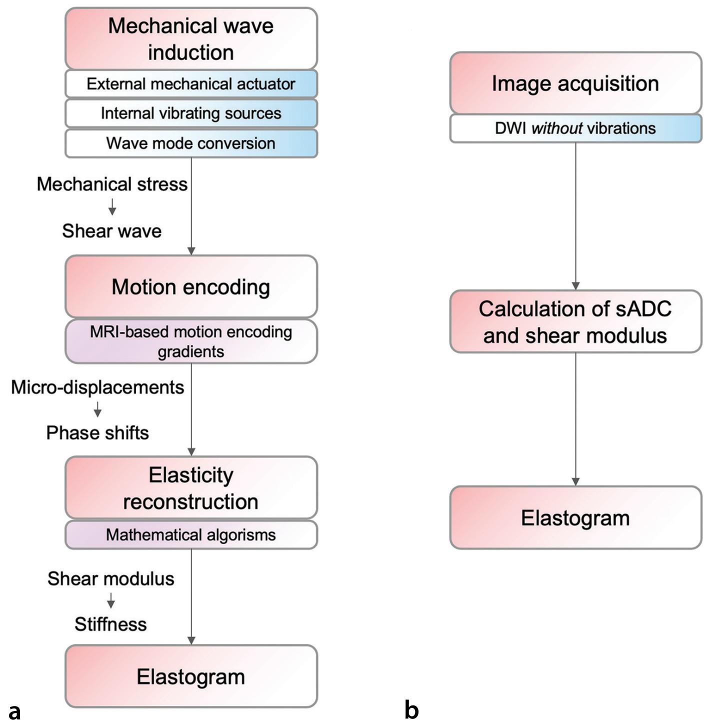


**Figure 4.** Mechanisms of magnetic resonance elastography and virtual magnetic resonance elastography for tumor stiffness mapping. **(a)** Flowchart illustrating the conventional magnetic resonance elastography (MRE) process (left), which involves mechanical wave induction, motion encoding, and elasticity reconstruction. **(b)** Virtual MRE workflow (right), which derives stiffness maps based on diffusion-weighted imaging without external vibration. DWI, diffusion-weighted imaging; sADC, shifted apparent diffusion coefficient; MRI, magnetic resonance imaging.

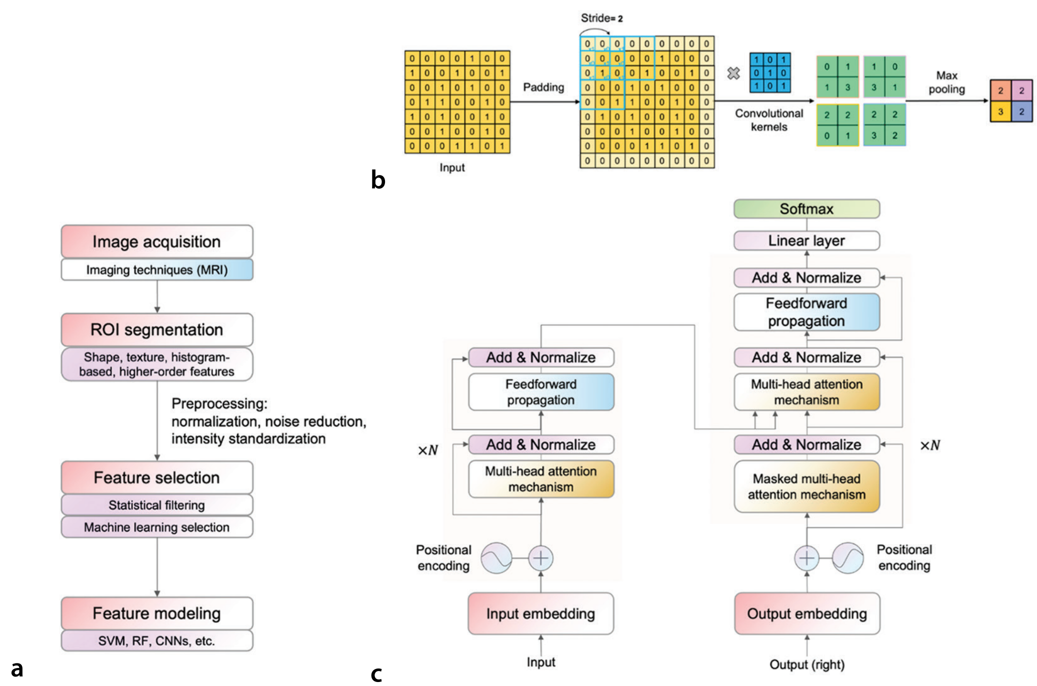


**Figure 5.** Machine learning architectures for magnetic resonance imaging-based prediction of pituitary adenoma consistency. **(a)** Workflow of conventional radiomics combined with traditional machine learning techniques. This includes magnetic resonance image acquisition, region of interest segmentation, feature extraction, and preprocessing (e.g., normalization and standardization), followed by feature selection and model construction using algorithms such as support vector machine and random forest. **(b)** A schematic of a convolutional neural network, illustrating convolution operations with kernel filters, stride, padding, and max pooling, which are used to extract spatial features from input images. Convolutional neural networks are capable of automatic feature extraction without handcrafted inputs. **(c)** Transformer model architecture, consisting of encoder and decoder blocks that incorporate multi-head self-attention and feedforward layers. Positional encoding and masked attention mechanisms allow the transformer to model long-range dependencies and global contextual relationships within the image data. Transformer frame diagram based on Vaswani et al.[65] ROI, region-of-interest; MRI, magnetic resonance imaging; SVM, support vector machine; RF, random forest; CNN, convolutional neural network.

outcomes. Common classifiers include decision trees, support vector machines (SVMs), k-nearest neighbors, naive Bayes, and logistic regression.

Classifiers are ML models designed to categorize data into predefined classes based on patterns learned from input features. These models operate through supervised learning, using labeled datasets to distinguish between tumor consistencies such as "soft" and "hard." Models such as SVMs and random forests (RFs) handle structured data, whereas deep-learning classifiers (e.g., CNNs) extract hierarchical features from raw images. These models enhance diagnostic accuracy, provide insights into tumor biology, and support preoperative evaluation and personalized treatment planning.

Notably, traditional ML classifiers have demonstrated considerable potential for predicting PA consistency (Table 3). RF is an ensemble learning algorithm that builds multiple decision trees during training. Each tree is trained on a random subset of features and data points, and their outputs are combined for classification. This approach effectively handles large, high-dimensional datasets, reduces overfitting, and captures complex variable interactions. SVMs classify data by identifying a hyperplane that best separates classes in feature space. Linear SVMs utilize a linear boundary, whereas kernel-based SVMs address non-linear relationships. Mendi et al.[56] applied both methods to T2-weighted features, achieving sensitivities of 95.58% and 92.95%, and specificities of 83.70% and 88.42%, respectively. Similarly, Wan et al.[57] used SVMs with > 300 T1- and T2-weighted MRI features, selecting 11 key features to build a model distinguishing hard from soft PMAs (AUC: 0.90, accuracy: 87%). ML models can further improve predictive performance by integrating imaging features with clinical variables. Fan et al.[58] developed an SVM model combining Knosp grade and radiomics features, obtaining AUCs of 0.83 in the training cohort and 0.81 in the validation cohort for patients with acromegaly. These classifiers effectively manage structured datasets and complex interactions, making them suitable for distinguishing soft from hard tumors.

The Extra Trees classifier, as used by Cuocolo et al.,[59] is similar to RF but introduces additional randomness through random threshold selection during feature splitting. This study employed the Extra Trees classifier on 1,118 texture features extracted from T2-weighted MRI data, achieving an accuracy of 93% and an AUC of 0.99, further highlighting the robustness of ensemble methods in this field.

Independent texture-based methods focus on specific radiomic features, such as contrast, entropy, and uniformity, to predict tumor consistency. These features are analyzed using simpler classifiers or statistical tests to evaluate predictive strength. Artzi et al.[60] applied ML to texture features derived from T2-weighted images and ADC maps, finding higher ADC values in vascular tumors and lower values in fibrous tumors, correlating with tumor heterogeneity and tissue organization.

Despite these promising findings, the overall evidence supporting MRI-based ML for PA consistency prediction remains preliminary. Most studies are retrospective and single-center, involve relatively small datasets, lack external validation, and have considerable risk of overfitting. In addition, variations in segmentation methods, feature extraction pipelines, class definitions, and outcome labeling reduce reproducibility. Clinically, high model performance alone does not guarantee readiness for routine implementation. Major barriers include limited interpretability, lack of standardized workflows, and uncertain generalizability across institutions and imaging platforms. Therefore, current ML models should be interpreted as proof-of-concept tools rather than clinically deployable systems. Future research should prioritize multicenter validation, standardized reporting, and enhanced interpretability. In this context, advanced methods such as deep learning classifiers—particularly CNNs—have emerged as promising due to their scalability and ability to learn hierarchical features from unstructured imaging data

**Table 3.** Studies using radiomics and machine learning to assess pituitary tumor consistency, from the year 2000 to the year 2024

| Author | Year | n | Imaging protocol | Model/Classifier/Statistical method | Training methods | Features extracted |
|---|---|---|---|---|---|---|
| **Mendi[56]** | 2023 | 52 | MRI T1, T2 | Random forest, support vector machine | Not reported | Not reported |
| **Wan[57]** | 2022 | 156 | MRI T1, T1CE, T2 | Random forest, support vector machine | 108 trained, 48 tested | 388 features |
| **Wang[63]** | 2021 | 213 | MRI T1, T1CE, T2 | Linear support vector classifier | 131 trained, 32 tested | 1197 features |
| **Zhu[62]** | 2020 | | MRI T1, T2 | Densely Connected Convolutional Network, Deep Residual Network, Convolutional Recurrent Neural Network | Not reported | Not reported |
| **Cuocolo[59]** | 2020 | 89 | MRI T2 | Extra Trees classifier | 5-fold cross-validation | 1118 features |
| **Fan[58]** | 2019 | 158 | MRI T1, T2, T1CE | Support vector machine | 100 trained, 58 tested | 1561 features |
| **Zeynalova[64]** | 2019 | 55 | MRI T1, T1CE, T2 | Artificial Neural Network | 10-fold cross-validation | 162 features |
| **Rui[76]** | 2019 | 53 | MRI T1, T1CE, CE 3D-T2 SPACE | Independent texture features | NA | 59 MR textural analysis features |
| **Sanei Taheri[77]** | 2019 | 32 | DWI | Kruskal-Wallis test | NA | First- and second-order histogram features on DWI |
| **Artzi[60]** | 2018 | 109 | MRI T1CE, T2 | Independent features | Not reported | 15 features based on T1- and T2-weighted MRI |

MRI, magnetic resonance imaging; DWI, diffusion-weighted imaging; T1CE, contrast-enhanced T1-weighted imaging; 3D, three-dimensional.

automatically. However, these models similarly require robust external validation and careful evaluation of clinical applicability.

### Application of convolutional neural networks technology in predicting pituitary adenoma consistency

A CNN is a type of feedforward neural network that automatically extracts features through convolution operations without relying on manually designed features.[61] In CNN architecture, convolutional kernels simulate neuronal receptive fields responding to various features, activation functions emulate neurons' threshold-response phenomena, and loss functions and optimizers fine-tune network performance. A CNN typically involves four essential components: convolution, padding, stride, and pooling. Convolution is the core step for feature extraction, producing feature maps. However, fixed-size convolutional kernels may cause boundary information loss. To address this, padding extends the input by adding zero values. Stride controls feature-map density, with larger strides yielding sparser maps. To reduce redundancy and prevent overfitting, pooling operations (max pooling and average pooling) are applied. Figure 5b illustrates a classic two-dimensional convolution process. To expand the receptive field, researchers introduced dilated convolution, significantly increasing receptive-field size without changing kernel dimensions, thereby enhancing feature capture. A key advantage of CNNs is their local connectivity and weight-sharing mechanisms, which substantially reduce parameter numbers and mitigate overfitting risk. Recently, CNNs have shown remarkable potential for predicting PA consistency.

Expanding on CNN principles, densely connected convolutional networks (DenseNets) enhance feature propagation and reuse by connecting each layer directly to all subsequent layers. This approach improves efficiency and reduces the vanishing gradient problem, making DenseNet ideal for image-based tasks. Recurrent neural networks (RNNs) extend deep learning to sequential data, capturing temporal dependencies useful in dynamic imaging and longitudinal studies. Zhu et al.[62] developed a semi-supervised pipeline employing CycleGAN and DenseNet–ResNet autoencoders to optimize feature extraction and classification in predicting tumor softness, achieving 91.78% accuracy despite limited MRI data. Wang et al.[63] further expanded this approach by implementing a gated-shaped U-Net for automatic segmentation of the sellar region into eight classes, extracting features such as tumor diameter, volume, and Knosp grade, and achieving AUCs of 0.84 and 0.92 for predicting tumor consistency.

Artificial neural networks (ANNs) mimic human brain structures, consisting of interconnected layers of nodes (neurons). Each neuron applies weights to inputs and passes results through activation functions, enabling the network to learn data patterns. ANNs are particularly suitable for smaller datasets with structured inputs, such as radiomic features, and often use feature selection methods to improve accuracy. Zeynalova et al.[64] demonstrated ANN effectiveness with 10-fold cross-validation on T2-weighted histogram features, achieving an AUC of 0.71 and outperforming traditional signal intensity ratio analysis.

However, although CNN-based models have demonstrated major value in the preoperative clinical planning of PAs, their limited capacity for modeling long-range dependencies restricts effective capture of global information. When handling medical images with complex morphological characteristics, focusing solely on local features cannot adequately fulfill comprehensive feature representation requirements. Therefore, these models must accurately represent global feature variations. Moreover, CNNs function as "black box" models, lacking transparency and explainability. This limitation is especially critical in medicine, where interpretability directly influences clinical decision-making reliability.

### Application of transformers and convolutional neural network–transformer combined technology in predicting pituitary adenoma consistency

Transformers, utilizing a self-attention mechanism and an encoder–decoder architecture, offer a promising approach for advancing preoperative predictions of PA consistency. Introduced by Vaswani et al.,[65] the transformer addresses inefficiencies of traditional RNNs, including difficulties in parallelization and challenges in capturing long-range dependencies. Transformers process sequential data via a self-attention mechanism, enabling each position in a sequence to interact directly with every other position, effectively modeling long-distance relationships.

The transformer adopts an encoder–decoder architecture. The encoder transforms an input sequence $(x_1, ..., x_n)$ into a continuous representation $z = (z_1, ..., z_n)$, and the decoder generates an output sequence $(y_1, ..., y_n)$ step-by-step in an autoregressive manner. Both the encoder and decoder contain six stacked layers, each comprising multiple sublayers. Encoder sublayers include (1) a multi-head self-attention mechanism, allowing simultaneous attention to different sequence parts, and (2) a feed-forward neural network that processes attention outputs. Each sublayer incorporates residual connections and layer normalization, computed as "LayerNorm(x+Sublayer(x))". The decoder structure resembles the encoder but adds an additional multi-head attention sublayer over the encoder outputs, facilitating encoder–decoder interaction. The left and right sections of Figure 5c illustrate encoder and decoder architectures, respectively. This design enables the transformer to capture relationships between sequence elements efficiently, making it highly effective in modern deep learning tasks.

Drawing inspiration from the transformer semantic-net (TS-Net), a deep learning architecture designed for voxel-level dose prediction in brain tumors,[66] transformers can leverage global feature extraction and semantic alignment to improve prediction accuracy in PAs. In TS-Net, the transformer encoder effectively captures long-range correlations across imaging modalities, and a semantic field alignment block ensures efficient propagation of high-level semantic information, yielding accurate voxel-level predictions. Such methodologies could be adapted for PMA consistency prediction by integrating multiple MRI modalities and clinical parameters, such as Knosp grade and collagen-related features.

Future research should focus on developing transformer-based architectures specifically tailored for PAs and combining transformers with traditional CNN-based models. CNNs excel at capturing local features, processing spatial information efficiently, and reducing computational costs. Conversely, transformers effectively model long-distance dependencies.[65] Combining these two methods would enable comprehensive image content analysis, effectively integrating detailed local information with global context.

Currently, a notable limitation across all MRI-based methods remains the lack of standardized acquisition and post-processing protocols. This limitation reduces reproducibility, complicates cross-study comparisons, and hampers multicenter validation efforts.

### Acknowledgements

The authors would like to express our heartfelt gratitude to Dr. Jian Ren (Xuanwu Hospital Capital Medical University) for his kind assistance in creating the schematic illustrations (a6 and b6) presented in Figure 2.

We are also deeply grateful to the patients featured in Figure 2 and Supplementary Figure 1, who generously consented to the use of their brain imaging, surgical photographs, and medical information for the purpose of this publication.


### Footnotes

### Conflict of interest disclosure

The authors declared no conflicts of interest.

**Supplementary Table:** https://d2v96fxpocvxx.cloudfront.net/beb8919b-f013-4ea1-b1c8-40332e840fe1/content-images/79246375-52e2-40c4-9e8c-f1c841b56933.pdf

**Supplementary Figure:** https://d2v96fxpocvxx.cloudfront.net/beb8919b-f013-4ea1-b1c8-40332e840fe1/content-images/17d5c607-0c67-45fe-aff7-c07bf9f3a2ac.pdf

## References


1. Molitch ME. Diagnosis and treatment of pituitary adenomas: a review. *JAMA*. 2017;317(5):516-524. [Crossref]
2. Fernandez A, Karavitaki N, Wass JA. Prevalence of pituitary adenomas: a community-based, cross-sectional study in Banbury (Oxfordshire, UK). *Clin Endocrinol (Oxf)*. 2010;72(3):377-382. [Crossref]
3. Cho DY, Liau WR. Comparison of endonasal endoscopic surgery and sublabial microsurgery for prolactinomas. *Surg Neurol*. 2002;58(6):371-375. [Crossref]
4. Cappabianca P, Cavallo LM, Colao A, et al. Endoscopic endonasal transsphenoidal approach: outcome analysis of 100 consecutive procedures. *Minim Invasive Neurosurg*. 2002;45(4):193-200. [Crossref]
5. Naganuma H, Satoh E, Nukui H. Technical considerations of transsphenoidal removal of fibrous pituitary adenomas and evaluation of collagen content and subtype in the adenomas. *Neurol Med Chir (Tokyo)*. 2002;42(5):202-212; discussion 213. [Crossref]
6. Černý M, Sedlák V, Lesáková V, Francůz P, Netuka D. Methods of preoperative prediction of pituitary adenoma consistency: a systematic review. *Neurosurg Rev*. 2022;46(1):11. [Crossref]
7. Yun JJ, Johans SJ, Shepherd DJ, et al. The utility of using preoperative MRI as a predictor for intraoperative pituitary adenoma consistency and surgical resection technique. *J Neurol Surg B Skull Base*. 2020;81(6):651-658. [Crossref]
8. Yildirim MS, Schmidbauer VU, Micko A, et al. Multi-dynamic-multi-echo-based MRI for the pre-surgical determination of sellar tumor consistency: a quantitative approach for predicting lesion resectability. *Clin Neuroradiol*. 2024;34:663-673. [Crossref]
9. Rutkowski MJ, Chang KE, Cardinal T, et al. Development and clinical validation of a grading system for pituitary adenoma consistency. *J Neurosurg*. 2020;134(6):1800-1807. [Crossref]
10. Acitores Cancela A, Rodríguez Berrocal V, Pian Arias H, Díez JJ, Iglesias P. Effect of pituitary adenoma consistency on surgical outcomes in patients undergoing endonasal endoscopic transsphenoidal surgery. *Endocrine*. 2022;78(3):559-569. [Crossref]
11. De Alcubierre D, Puliani G, Cozzolino A, et al. Pituitary adenoma consistency affects postoperative hormone function: a retrospective study. *BMC Endocr Disord*. 2023;23:92. [Crossref]
12. Li P, Zhang D, Ma S, et al. Consistency of pituitary adenomas: amounts of collagen types I and III and the predictive value of T2WI MRI. *Exp Ther Med*. 2021;22(5):1255. [Crossref]
13. Yao A, Rutland JW, Verma G, et al. Pituitary adenoma consistency: direct correlation of ultrahigh field 7T MRI with histopathological analysis. *Eur J Radiol*. 2020;126:108931. [Crossref]
14. Nachtigall LB, Karavitaki N, Kiseljak-Vassiliades K, et al. Physicians' awareness of gadolinium retention and MRI timing practices in the longitudinal management of pituitary tumors: a "Pituitary Society" survey. *Pituitary*. 2019;22(1):37-45. [Crossref]
15. Knosp E, Steiner E, Kitz K, Matula C. Pituitary adenomas with invasion of the cavernous sinus space: a magnetic resonance imaging classification compared with surgical findings. *Neurosurgery*. 1993;33(4):610-617; discussion 617-618. [Crossref]
16. Micko AS, Wöhrer A, Wolfsberger S, Knosp E. Invasion of the cavernous sinus space in pituitary adenomas: endoscopic verification and its correlation with an MRI-based classification. *J Neurosurg*. 2015;122(4):803-811. [Crossref]
17. De Araujo e Silva JL, Araujo e Silva GQ, Pereira Portela G, et al. Soft or firm pituitary adenoma? How to assist the neurosurgeon. In: European Congress of Radiology (ECR 2017); 2017 Mar 1–5; Vienna, Austria. *Insights Imaging*. 2017;8(Suppl 1). [Crossref]
18. Bashari WA, Senanayake R, Fernández-Pombo A, et al. Modern imaging of pituitary adenomas. *Best Pract Res Clin Endocrinol Metab*. 2019;33(2):101278. [Crossref]
19. Mastorakos P, Mehta GU, Chatrath A, et al. Tumor to cerebellar peduncle T2-weighted imaging intensity ratio fails to predict pituitary adenoma consistency. *J Neurol Surg B Skull Base*. 2019;80(3):252-257. [Crossref]
20. Chen XY, Ding CY, You HH, et al. Relationship between pituitary adenoma consistency and extent of resection based on tumor/cerebellar peduncle T2-weighted imaging intensity (TCTI) ratio of the point on preoperative magnetic resonance imaging (MRI) corresponding to the residual point on postoperative MRI. *Med Sci Monit*. 2020;26:e919565. [Crossref]
21. Wei L, Lin SA, Fan K, Xiao D, Hong J, Wang S. Relationship between pituitary adenoma texture and collagen content revealed by comparative study of MRI and pathology analysis. *Int J Clin Exp Med*. 2015;8(8):12898-12905. [Crossref]
22. Smith KA, Leever JD, Chamoun RB. Prediction of consistency of pituitary adenomas by magnetic resonance imaging. *J Neurol Surg B Skull Base*. 2015;76(5):340-343. [Crossref]
23. Yamamoto J, Kakeda S, Shimajiri S, et al. Tumor consistency of pituitary macroadenomas: predictive analysis on the basis of imaging features with contrast-enhanced 3D FIESTA at 3T. *AJNR Am J Neuroradiol*. 2014;35(2):297-303. [Crossref]
24. Hagmann P, Jonasson L, Maeder P, Thiran JP, Wedeen VJ, Meuli R. Understanding diffusion MR imaging techniques: from scalar diffusion-weighted imaging to diffusion tensor imaging and beyond. *Radiographics*. 2006;26 Suppl 1:S205- S223. [Crossref]
25. Iima M, Le Bihan D. Clinical intravoxel incoherent motion and diffusion MR imaging: past, present, and future. *Radiology*. 2016;278(1):13-32. [Crossref]
26. Le Bihan D. Apparent diffusion coefficient and beyond: what diffusion MR imaging can tell us about tissue structure. *Radiology*. 2013;268(2):318-322. [Crossref]
27. Moritani T, Ekholm S, Westesson PL, editors. Diffusion-weighted MR imaging of the brain. Berlin: Springer; 2005. [Crossref]
28. Ding W, Huang Z, Zhou G, Li L, Zhang M, Li Z. Diffusion-weighted imaging for predicting tumor consistency and extent of resection in patients with pituitary adenoma. *Neurosurg Rev*. 2021;44(5):2933-2941. [Crossref]
29. Rutland JW, Loewenstern J, Ranti D, et al. Analysis of 7-tesla diffusion-weighted imaging in the prediction of pituitary macroadenoma consistency. *J Neurosurg*. 2021;134(3):771-779. [Crossref]
30. Su CQ, Zhang X, Pan T, et al. Texture analysis of high b-value diffusion-weighted imaging for evaluating consistency of pituitary macroadenomas. *J Magn Reson Imaging*. 2020;51(5):1507-1513. [Crossref]

31. Pierallini A, Caramia F, Falcone C, et al. Pituitary macroadenomas: preoperative evaluation of consistency with diffusion-weighted MR imaging--initial experience. *Radiology*. 2006;239(1):223-231. [Crossref]

32. Mohamed FF, Aboulhashem S. Diagnostic value of apparent diffusion coefficient (ADC) in assessment of pituitary macroadenoma consistency. *Egypt J Radiol Nucl Med*. 2013;44(3):617-624. [Crossref]

33. Alashwah MA, Moharram MA, Allakany AS. Role of diffusion weighted magnetic resonance imaging (DW-MRI) in choice of the surgical approach for pituitary macroadenoma resection. *Egypt J Radiol Nucl Med*. 2017;48(4):983-989. [Crossref]

34. Thomas T, Gopalakrishnan CV, Thomas B, Nair S. Evaluation of consistency of pituitary macroadenoma using diffusion-weighted imaging in correlation with surgical findings. *Neurosurg Q*. 2014;24(2):131-135. [Crossref]

35. Taghvaei M, Tajik F, Zeinalizadeh M, Azmoudeh Ardalan F, Ghanaati H. Is there any congruity between tumor consistency in pituitary macroadenomas and preoperative diffusion weighted imaging and apparent diffusion coefficient (ADC) map? *Arch Neurosci*. 2017;4(4):e14553. [Crossref]

36. Barbosa MA, Pereira EGR, da Mata Pereira PJ, et al. Diffusion-weighted imaging does not seem to be a predictor of consistency in pituitary adenomas. *Pituitary*. 2024;27(2):187-196. [Crossref]

37. Suzuki C, Maeda M, Hori K, et al. Apparent diffusion coefficient of pituitary macroadenoma evaluated with line-scan diffusion-weighted imaging. *J Neuroradiol*. 2007;34(4):228-235. [Crossref]

38. Kamimura K, Nakajo M, Bohara M, et al. Consistency of pituitary adenoma: prediction by pharmacokinetic dynamic contrast-enhanced MRI and comparison with histologic collagen content. *Cancers (Basel)*. 2021;13(15):3914. [Crossref]

39. Cohen-Cohen S, Helal A, Yin Z, et al. Predicting pituitary adenoma consistency with preoperative magnetic resonance elastography. *J Neurosurg*. 2021;136(5):1356-1363. [Crossref]

40. Garg M, Sridhar MS, Verma S, Bhadoria J. Clinical outcomes based on intraoperative consistency of tumors and apparent diffusion coefficient value in pituitary macroadenoma post-endoscopic transsphenoidal excision. *Indian J Appl Res*. 2019;9(1). [Crossref]

41. Yiping L, Ji X, Daoying G, Bo Y. Prediction of the consistency of pituitary adenoma: a comparative study on diffusion-weighted imaging and pathological results. *J Neuroradiol*. 2016;43(3):186-194. [Crossref]

42. Mahmoud OM, Tominaga A, Amatya VJ, et al. Role of PROPELLER diffusion-weighted imaging and apparent diffusion coefficient in the evaluation of pituitary adenomas. *Eur J Radiol*. 2011;80(2):412-417. [Crossref]

43. Le Bihan D, Breton E, Lallemand D, Aubin ML, Vignaud J, Laval-Jeantet M. Separation of diffusion and perfusion in intravoxel incoherent motion MR imaging. *Radiology*. 1988;168(2):497-505. [Crossref]

44. Su CQ, Wang BB, Tang WT, et al. Diffusion-relaxation correlation spectrum imaging for predicting tumor consistency and gross total resection in patients with pituitary adenomas: a preliminary study. *Eur Radiol*. 2023;33(10):6993-7002. [Crossref]

45. Wang M, Liu H, Wei X, et al. Application of reduced-FOV diffusion-weighted imaging in evaluation of normal pituitary glands and pituitary macroadenomas. *AJNR Am J Neuroradiol*. 2018;39(8):1499-1504. [Crossref]

46. Khant ZA, Azuma M, Kadota Y, et al. Evaluation of pituitary structures and lesions with turbo spin-echo diffusion-weighted imaging. *J Neurol Sci*. 2019;405:116390. [Crossref]

47. Hughes JD, Fattahi N, Van Gompel J, Arani A, Ehman R, Huston J 3rd. Magnetic resonance elastography detects tumoral consistency in pituitary macroadenomas. *Pituitary*. 2016;19(3):286-292. [Crossref]

48. Sakai N, Takehara Y, Yamashita S, et al. Shear stiffness of 4 common intracranial tumors measured using MR elastography: comparison with intraoperative consistency grading. *AJNR Am J Neuroradiol*. 2016;37(10):1851-1859. [Crossref]

49. Bao Y, Qiu S, Li Z, Yang G, Feng Y, Yue Q. Preoperative assessment of meningioma consistency using a combination of MR elastography and DTI. *AJNR Am J Neuroradiol*. 2024. [Crossref]

50. Lagerstrand K, Gaedes N, Eriksson S, et al. Virtual magnetic resonance elastography has the feasibility to evaluate preoperative pituitary adenoma consistency. *Pituitary*. 2021;24(4):530-541. [Crossref]

51. Aunan-Diop JS, Halle B, Pedersen CB, et al. Magnetic resonance elastography in intracranial neoplasms: a scoping review. *Top Magn Reson Imaging*. 2022;31(1):9-22. [Crossref]

52. Le Bihan D, Ichikawa S, Motosugi U. Diffusion and intravoxel incoherent motion MR imaging-based virtual elastography: a hypothesis-generating study in the liver. *Radiology*. 2017;285(2):609-619. [Crossref]

53. Ota T, Hori M, Le Bihan D, et al. Diffusion-based virtual MR elastography of the liver: can it be extended beyond liver fibrosis? *J Clin Med*. 2021;10(19):4553. [Crossref]

54. Jung HN, Ryoo I, Suh S, Lee YH, Kim E. Evaluating the elasticity of metastatic cervical lymph nodes in head and neck squamous cell carcinoma patients using DWI-based virtual MR elastography. *Magn Reson Med Sci*. 2024;23(1):49-55. [Crossref]

55. Zheng B, Zhao Z, Zheng P, et al. The current state of MRI-based radiomics in pituitary adenoma: promising but challenging. *Front Endocrinol (Lausanne)*. 2024;15:1426781. [Crossref]

56. Mendi BAR, Batur H, Çay N, Çakır BT. Radiomic analysis of preoperative magnetic resonance imaging for the prediction of pituitary adenoma consistency. *Acta Radiol*. 2023;64(8):2470-2478. [Crossref]

57. Wan T, Wu C, Meng M, et al. Radiomic features on multiparametric MRI for preoperative evaluation of pituitary macroadenomas consistency: preliminary findings. *J Magn Reson Imaging*. 2022;55(5):1491-1503. [Crossref]

58. Fan Y, Hua M, Mou A, et al. Preoperative noninvasive radiomics approach predicts tumor consistency in patients with acromegaly: development and multicenter prospective validation. *Front Endocrinol (Lausanne)*. 2019;10:403. [Crossref]

59. Cuocolo R, Ugga L, Solari D, et al. Prediction of pituitary adenoma surgical consistency: radiomic data mining and machine learning on T2-weighted MRI. *Neuroradiology*. 2020;62(12):1649-1656. [Crossref]

60. Artzi M, Shofty B, Kashanian A, et al. COMP-23. Assessment of pituitary adenoma consistency and vascularity using texture analysis of conventional MRI. *Neuro Oncol*. 2018;20(Suppl 6):vi68. [Crossref]

61. Li Z, Liu F, Yang W, Peng S, Zhou J. A survey of convolutional neural networks: analysis, applications, and prospects. *IEEE Trans Neural Netw Learn Syst*. 2022;33(12):6999-7019. [Crossref]

62. Zhu H, Fang Q, Huang Y, Xu K. Semi-supervised method for image texture classification of pituitary tumors via CycleGAN and optimized feature extraction. *BMC Med Inform Decis Mak*. 2020;20(1):215. [Crossref]

63. Wang H, Zhang W, Li S, Fan Y, Feng M, Wang R. Development and evaluation of deep learning-based automated segmentation of pituitary adenoma in clinical task. *J Clin Endocrinol Metab*. 2021;106(9):2535-2546. [Crossref]

64. Zeynalova A, Kocak B, Durmaz ES, et al. Preoperative evaluation of tumour consistency in pituitary macroadenomas: a machine learning-based histogram analysis on conventional T2-weighted MRI. *Neuroradiology*. 2019;61(7):767-774. [Crossref]

65. Vaswani A, Shazeer N, Parmar N, et al. Attention is all you need. *arXiv*. 2017;arXiv:1706.03762. [Crossref]

66. Yang J, Zhao Y, Zhang F, Liao M, Yang X. Deep learning architecture with transformer and semantic field alignment for voxel-level dose prediction on brain tumors. *Med Phys*. 2023;50(2):1149-1161. [Crossref]

67. Baban MIA, Omer SN, AlZuhairy AKA, Mahmoud AA. The role of preoperative MRI in endoscopic transnasal transsphenoidal hypophysectomy of pituitary adenoma. *Eur Arch Otorhinolaryngol.* 2024;281(4):1961-1969. [Crossref]

68. Gaia F, Filho JRMC, Reyes LCMG, et al. Predictive assessment of the consistency of pituitary adenomas using signal intensity in magnetic resonance imaging and fractal dimension of histopathological features [Preprint]. *Research Square.* 2022. [Crossref]

69. Cappelletti M, Ruggeri AG, Spizzichino L, D'Amico A, D'avella E, Delfini R. Fibrous pituitary macroadenomas: predictive role of preoperative radiologic investigations for proper surgical planning in a cohort of 66 patients. *World Neurosurg*. 2019;121:e449-e457. [Crossref]

70. Thotakura AK, Patibandla MR, Panigrahi MK, Mahadevan A. Is it really possible to predict the consistency of a pituitary adenoma preoperatively? *Neurochirurgie*. 2017;63(6):453-457. [Crossref]

71. Alimohamadi M, Sanjari R, Mortazavi A, et al. Predictive value of diffusion-weighted MRI for tumor consistency and resection rate of nonfunctional pituitary macroadenomas. *Acta Neurochir (Wien)*. 2014;156(12):2245-2252; discussion 2252. [Crossref]

72. Boxerman JL, Rogg JM, Donahue JE, Machan JT, Goldman MA, Doberstein CE. Preoperative MRI evaluation of pituitary macroadenoma: imaging features predictive of successful transsphenoidal surgery. *AJR Am J Roentgenol.* 2010;195(3):720-728. [Crossref]

73. Bahuleyan B, Raghuram L, Rajshekhar V, Chacko AG. To assess the ability of MRI to predict consistency of pituitary macroadenomas. *Br J Neurosurg*. 2006;20(5):324-326. [Crossref]

74. Hagiwara A, Inoue Y, Wakasa K, Haba T, Tashiro T, Miyamoto T. Comparison of growth hormone-producing and non-growth hormone-producing pituitary adenomas: imaging characteristics and pathologic correlation. *Radiology*. 2003;228(2):533-538. [Crossref]

75. Alimohamadi M, Sanjari R, Shirani M, Alikhani F, Amirjamshidi A. Initial experience with diffusion-weighted imaging to predict the tumor consistency and surgical success in solid growth hormone producing pituitary macroadenomas. *Asian J Neurosurg.* 2019;14(3):698-701. [Crossref]

76. Rui W, Wu Y, Ma Z, et al. MR textural analysis on contrast enhanced 3D-SPACE images in assessment of consistency of pituitary macroadenoma. *Eur J Radiol.* 2019;110:219-224. [Crossref]

77. Sanei Taheri M, Kimia F, Mehrnahad M, et al. Accuracy of diffusion-weighted imaging-magnetic resonance in differentiating functional from non-functional pituitary macro-adenoma and classification of tumor consistency. *Neuroradiol J.* 2019;32(2):74-85. [Crossref]

78. Koh DM, Collins DJ. Diffusion-weighted MRI in the body: applications and challenges in oncology. *AJR Am J Roentgenol.* 2007;188(6):1622-1635. [Crossref]